A Posteriori Finite Element Error Bounds for Nonlinear Outputs of the Helmholtz Equation

J. Sarrate [*], J. Peraire [†] and A. Patera [‡]

June 1, 1999

Abstract

We present a Neumann–subproblem *a posteriori* finite element procedure for the efficient and accurate calculation of rigorous, constant–free upper and lower bounds for nonlinear outputs of the Helmholtz equation in two–dimensional exterior domains. We first formulate the bound procedure, with particular emphasis on appropriate extension to complex–valued equations; we then provide illustrative numerical examples for outputs such as the intensity of the scattered wave over a small segment of the domain boundary.

1 Introduction

In the last two decades, engineering applications that involve the solution of the Helmholtz equation in exterior domains — scattering wave problems — have become increasingly important. These applications range from low–frequency problems such as sea–wave propagation in inner ports [15], to high–frequency problems such as the prediction of the radar scattering cross–section of complex objects and vehicles [9, 27, 28].

Several numerical techniques can be used to solve these challenging problems. For homogeneous media, boundary integral methods [4, 10, 14] are probably the most prevalent. These techniques automatically satisfy the radiation condition at infinity; furthermore, they reduce the effective spatial dimension of the problem, which in turn leads to significant computational economies. However, recent developments in the field of approximate boundary conditions, infinite elements, and iterative solvers [8, 12, 25] have rendered the finite element method competitive, especially for nonhomogeneous media. Critical questions remain, however, in particular as regards accuracy and appropriate meshes.

In general, the accuracy of a finite element solution of a partial differential equation can be predicted by *a priori* and *a posteriori* error estimators. *A priori* error estimates can be readily found even for noncoercive problems such as the Helmholtz equation in, for example, the H^1 and L^2 norms [26, 27]. Although these estimates reveal the correct asymtotic rate of convergence, their application to practical computations is limited since the estimates involve norms of the unknown solution. *A posteriori* procedures overcome this problem by expressing the error in terms of the

[*]Work performed at: Department of Aeronautics and Astronautics, Massachusetts Institute of Technology. Current address: Department de Matemàtica Aplicada III, Universitat Politècnica de Catalunya, Gran Capitan s/n, Modul C2, Barcelona, 08034, Spain. Corresponding author.

[†]Department of Aeronautics and Astronautics, Massachusetts Institute of Technology, Cambridge, MA 02139, USA.

[‡]Department of Mechanical Engineering, Massachusetts Institute of Technology, Cambridge, MA 02139, USA.

computed numerical solution. *A posteriori* error estimators in the H^1 and L^2 norms are available for the Helmholtz equation [5, 13, 28]; these estimators form the basis for effective adaptive procedures.

However, from the engineering point of view, it is more advantageous and interesting to develop *a posteriori* estimators for error metrics more directly relevant to engineering analysis. In particular, the quantity (or quantities) of interest in engineering studies is typically not the field variable u or the error in the energy norm, but rather the outputs (e.g. the flux across a boundary, the normal force on a surface, or the mean value of the solution) that reflect the specific goals and objectives of the design or optimization process. Moreover, engineers may be at least as interested in prediction confirmation as in adaptivity: it is thus essential that all constants be evaluated, and explicit techniques [7] are therefore less attractive than implicit procedures.

In [19, 20, 22, 23] we develop a general formulation for *a posteriori* bounds for output functionals of rather general partial differential equations. This formulation relies on previous developments in implicit (subproblem) *a posteriori* theory, in particular the application of quadratic–linear duality theory [6, 2] and the construction of equilibrated hybrid fluxes [2, 6, 16]. However, the critical discriminator and advantage of our approach is that we obtain rigorous, accurate, and quantitative (constant–free) bounds directly for the engineering quantities of interest, rather than the energy norm or energy–norm equivalents [3].

We initially applied our formulation to symmetric and coercive problems (the Poisson equation and linear elasticity) [22], nonsymmetric coercive problems (e.g. the convection–difussion equation), [22], certain constrained problems (e.g. the Stokes equations) [21], and noncoercive problems that satisfy a Gårding inequality [26] (e.g. the Helmholtz equation for interior domains) [24]. Recently, we have developed a more general formulation [19, 17] which not only includes these previous cases, but also nonlinear outputs and nonlinear equations (e.g. the eigenvalue problem, and the Burgers equation). Our goal in this paper is to extend our earlier work for the one–dimensional real–valued interior Helmholtz problem to the much more challenging, and relevant, multidimensional complex–valued exterior Helmholtz problem. We shall restrict our attention here to confirmation of (nonlinear) outputs: future papers will consider the development of local error indicators and associated adaptive strategies following the formulation described in [23].

This paper is organized as follows. In Section 2, the strong and the weak form of the problem are stated. In Section 3, several space definitions are introduced; the bound estimator procedure is then described; and, finally, the requisite bounding properties are demonstrated. In Section 4, several numerical examples are presented; brief conclusions are given in Section 5.

2 Problem Statement

2.1 Strong Formulation

Given an incident wave, we are interested in the computation of outputs which are nonlinear functionals of the resulting scattered wave. The strong form for the scattered wave in a homogeneous medium can be stated as: find $\tilde{u} : \bar{\Omega} \to \mathbb{R}$ such that

$$\begin{aligned} \frac{1}{c^2}\frac{\partial^2 \tilde{u}}{\partial t^2} - \nabla^2 \tilde{u} &= \tilde{f} && \text{in} \quad \Omega, && (1)\\ \tilde{u} &= \tilde{g}^D && \text{on} \quad \Gamma_D, && (2)\\ \frac{\partial \tilde{u}}{\partial n} &= \tilde{g}^N && \text{on} \quad \Gamma_N, && (3)\\ \frac{\partial \tilde{u}}{\partial n} &= -\frac{1}{c}\frac{\partial \tilde{u}}{\partial t} && \text{on} \quad \Gamma_R, && (4) \end{aligned}$$

where c is the wave velocity, $\tilde{f} : \bar{\Omega} \to \mathbb{R}$ is the source term, and $\tilde{g}^D : \Gamma_D \to \mathbb{R}$ and $\tilde{g}^N : \Gamma_N \to \mathbb{R}$ are Dirichlet and Neumann data, respectively; here $\partial\tilde{u}/\partial n = \nabla\tilde{u}\cdot\hat{\mathbf{n}}$, where $\hat{\mathbf{n}}$ is the outward unit normal on the boundary. It is important to note that our radiation condition on Γ_R is only approximate; higher order forms can be developed, but will not be pursued in this paper. We assume that the boundary Γ verifies

$$\Gamma = \overline{\Gamma_D \cup \Gamma_N \cup \Gamma_R} \tag{5}$$
$$\emptyset = \Gamma_D \cap \Gamma_N = \Gamma_D \cap \Gamma_R = \Gamma_N \cap \Gamma_R, \tag{6}$$

as shown in Figure 1.

Assuming harmonic data of the form $\tilde{f} = \Re\{f\ e^{i\omega t}\}$, $\tilde{g}^D = \Re\{g^D e^{i\omega t}\}$, and $\tilde{g}^N = \Re\{g^N e^{i\omega t}\}$ (where $\Re\{v\}$ denotes the real part of v, and $i = \sqrt{-1}$), the *stationary* solution of the above problem will be of the form $\tilde{u} = \Re\{u\ e^{i\omega t}\}$. The strong statement for the resulting complex Helmholtz equation is thus: find $u : \bar{\Omega} \to \mathbb{C}$ such that

$$-\nabla^2 u - k^2 u = f \qquad \text{in} \quad \Omega, \tag{7}$$
$$u = g^D \qquad \text{on} \quad \Gamma_D, \tag{8}$$
$$\frac{\partial u}{\partial n} = g^N \qquad \text{on} \quad \Gamma_N, \tag{9}$$
$$\frac{\partial u}{\partial n} = -i\ k\ u \qquad \text{on} \quad \Gamma_R, \tag{10}$$

where $k = \omega/c$ is the wave number. We evaluate our output s as a functional of the field variable u; this is described in greater detail in the next subsection.

2.2 Weak Formulation

We first introduce the space

$$\tilde{Z}(\mathcal{D}) = \left\{ v = v^R + iv^I \ : \ v^R \in H^1(\mathcal{D}),\ v^I \in H^1(\mathcal{D}) \right\}, \tag{11}$$

where $H^1(\mathcal{D})$ is the usual Sobolev space [1] associated with a domain $\mathcal{D} \subset \mathbb{R}^2$. Here and throughout this paper superscript R and I denote the real and imaginary part, respectively, that is, $v^R = \Re(v)$ and $v^I = \Im(v)$; $\overline{v}$ shall denote the complex conjugate of v, and $|v|$ the modulus of v. We then introduce the sets

$$Z = \left\{ v \in \tilde{Z}(\Omega) : \ v|_{\Gamma_D} = 0 \right\}, \tag{12}$$
$$Z^D = \left\{ v \in \tilde{Z}(\Omega) : \ v|_{\Gamma_D} = g^D \right\}, \tag{13}$$

which reflect the essential boundary conditions.

Under these definitions, the weak formulation of the Helmholtz problem is: find $u \in Z^D$ such that

$$\mathcal{A}(u, v) = 0, \qquad \forall v \in Z, \tag{14}$$

where the form $\mathcal{A} : \ \tilde{Z}(\Omega) \times \tilde{Z}(\Omega) \to \mathbb{C}$ is defined as

$$\mathcal{A}(u, v) = a(u, v) - m(u, v) + i\ p(u, v) - \langle f, v\rangle - \langle g^N, v\rangle_N. \tag{15}$$

Here the bilinear forms are given by

$$a(w,v) = \int_\Omega \nabla w \cdot \nabla \overline{v} \; d\Omega, \tag{16}$$

$$m(w,v) = k^2 \int_\Omega w\overline{v} \; d\Omega, \tag{17}$$

$$p(w,v) = k \int_{\Gamma_R} w\overline{v} \; d\Gamma, \tag{18}$$

and the duality pairings by (assuming sufficient smoothness)

$$\langle f, v\rangle = \int_\Omega f\overline{v} \; d\Omega, \tag{19}$$

$$\langle g^N, v\rangle_N = \int_{\Gamma_N} g^N\overline{v} \; d\Gamma. \tag{20}$$

We note that $a(\cdot,\cdot)$ is Hermitian positive–definite.

Finally, we are interested in real outputs, s, that are nonlinear functionals of the solution $u = u^R + i\, u^I$. More precisely, we set: $s = \Re\{S(u)\}$, where $S(u) : \tilde{Z}(\Omega) \rightarrow \mathbb{C}$. Specific examples will be presented later in the paper.

3 Error Bound Formulation

In this section we present a procedure to obtain sharp bound estimators for nonlinear outputs of the complex Helmholtz equation. In particular, we extend the general formulation developed in [19, 20, 22, 23] to the complex–valued case.

3.1 Space Definitions

We first introduce the finite element approximation subspaces. For our error bound procedure we consider two triangulations of Ω: a working mesh $\mathcal{T}_H$, and a truth mesh $\mathcal{T}_h$. We require that $\mathcal{T}_h$ is a refinement of $\mathcal{T}_H$ in the sense that any element, T_h, of $\mathcal{T}_h$ lies entirely within a single element, T_H, of $\mathcal{T}_H$. We can then define the standard piecewise-linear finite element sets

$$Z_\delta = \Big\{ v = v^R + i\, v^I \;:\; v^R|_{T_\delta} \in \mathbf{P}_1(T_\delta),\; v^I|_{T_\delta} \in \mathbf{P}_1(T_\delta),\; \forall T_\delta \in \mathcal{T}_\delta \Big\} \cap Z, \tag{21}$$

$$Z_\delta^D = \Big\{ v = v_R + i\, v^I \;:\; v^R|_{T_\delta} \in \mathbf{P}_1(T_\delta),\; v^I|_{T_\delta} \in \mathbf{P}_1(T_\delta),\; \forall T_\delta \in \mathcal{T}_\delta \Big\} \cap Z^D, \tag{22}$$

where $\mathbf{P}_1(T_\delta)$ is the space of linear polynomials over element T_δ. The working discretization corresponds to $\delta = H$ whereas the truth discretization corresponds to $\delta = h$. Note that $Z_H \subset Z_h \subset Z$, and furthermore $Z_H^D \subset Z_h^D \subset Z^D$ (we assume that g^D is sufficiently simple).

We can then find our working approximation, $u_H \in Z_H^D$, from

$$\mathcal{A}(u_H, v) = 0, \qquad \forall v \in Z_H, \tag{23}$$

and thus $s_H = \Re\{S(u_H)\}$. Similarly, for our truth mesh, $u_h \in Z_h^D$ satisfies

$$\mathcal{A}(u_h, v) = 0, \qquad \forall v \in Z_h, \tag{24}$$

with $s_h = \Re\{S(u_h)\}$. We assume that problem (23) can be solved at modest cost. We further assume that Z_h (the truth discretization) is sufficiently fine that s_h differs negligibly from s; this suggests that direct computation of s_h will be prohibitively expensive — hence the interest in bounds.

In order to apply the error bound procedure developed in [19, 22, 23] we need to define additional spaces and bilinear forms. First, we define the *broken* spaces with respect to the domain decomposition induced by Z_H as

$$\hat{Z}_\delta = \left\{ v|_{T_H} \in \tilde{Z}(T_H),\ \forall T_H \in \mathcal{T}_H :\ v^R|_{T_\delta} \in \mathbf{P}_1(T_\delta),\ v^I|_{T_\delta} \in \mathbf{P}_1(T_\delta),\ \forall T_\delta \in \mathcal{T}_\delta \right\}. \tag{25}$$

Second, we denote by $\mathcal{E}(\mathcal{T}_H)$ the set of open edges of the triangulation $\mathcal{T}_H$, and introduce a space of functions defined over the element edges $\gamma \in \mathcal{E}(\mathcal{T}_H)$,

$$\begin{aligned} \mathcal{Q}_H = \Big\{ q = q^R + i\ q^I \quad : \quad & q^R|_\gamma \in \mathbf{P}_1(\gamma),\ q^I|_\gamma \in \mathbf{P}_1(\gamma),\ \forall \gamma \in \mathcal{E}(\mathcal{T}_H), \\ & \text{and}\ \ q|_{\Gamma_N} = q|_{\Gamma_R} = 0 \Big\}. \end{aligned} \tag{26}$$

Finally, we define the continuity bilinear form as $b : \hat{Z}_h \times \mathcal{Q}_H \to \mathbb{C}$ as

$$b(v,q) = \sum_{\gamma \in \mathcal{E}(\mathcal{T}_H)} \int_\gamma [\bar{v}]_\gamma\ q|_\gamma\ d\Gamma, \tag{27}$$

where $[v]_\gamma$ is the jump in v across γ when γ is in the interior, and the trace of v on γ when γ is on the boundary Γ. It is important to note that the form $b(\cdot,\cdot)$ can be exploited to enforce continuity for example,

$$Z_H = \left\{ v \in \hat{Z}_H\ :\ b(v,q) = 0,\ \forall q \in \mathcal{Q}_H \right\}. \tag{28}$$

Conversely, for any continuous function v which satisfies the homogeneous essential boundary conditions, and any function $q \in \mathcal{Q}_H$, $b(v,q) = 0$.

3.2 Bound Procedure

Our goal is to find, based solely on computations on the working space Z_H and *decoupled calculations* on the *broken* space $\hat{Z}_h$, lower and upper estimators that provide lower and upper bounds for $S(u_h)$ for H sufficiently small.

We first define

$$E(w,v) \equiv a(w,v) - m(w,v) + i\ p(w,v); \tag{29}$$

we then further decompose E into its Hermitian and skew–Hermitian parts, $E = E^s + E^a$,

$$E^s(w,v) \equiv \frac{1}{2}\{E(w,v) + \overline{E(v,w)}\} = a(w,v) - m(w,v), \tag{30}$$

$$E^a(w,v) \equiv \frac{1}{2}\{E(w,v) - \overline{E(v,w)}\} = i\ p(w,v); \tag{31}$$

finally, the Hermitian part is decomposed as $E^s \equiv E^s_Y + E^s_M$, where

$$E^s_Y(w,v) \equiv a(w,v), \tag{32}$$

$$E^s_M(w,v) \equiv -m(w,v). \tag{33}$$

Note that $E^s_Y(\cdot,\cdot)$ is positive–definite.

For the purpuses of this paper, we shall restrict our attention to linear and quadratic outputs; more general nonlinear forms are readily treated, as described in [19]. We may thus expand our nonlinear output functional as

$$S(u_H + w) = S(u_H) + \ell^{\mathcal{O}}(w) + \mathcal{M}(w, w), \tag{34}$$

where $\ell^{\mathcal{O}} : \tilde{Z}(\Omega) \to \mathbb{C}$, and $\mathcal{M} : \tilde{Z}(\Omega) \times \tilde{Z}(\Omega) \to \mathbb{C}$ are the linear and bilinear contributions, respectively [19]. We shall require that $\mathcal{M}$ be L^2–continuous, in particular $|\mathcal{M}(w,w)| \leq C \parallel w \parallel_0^2$, where $\parallel \cdot \parallel_0$ denotes the L^2 norm. Note that for linear outputs, $\mathcal{M} = 0$.

The error bound procedure comprises the following five steps (for an alternative description see the Appendix).

Step 1. In the first step we compute the Galerkin finite element solution on the working mesh: find $u_H = u_H^R + i\ u_H^I \in Z_H^D$ such that

$$E(u_H, v) \;=\; \langle f, v\rangle + \langle g^N, v\rangle_N, \quad \forall v \in Z_H. \tag{35}$$

We also define the residual

$$R^u(v) \equiv \langle f, v\rangle + \langle g^N, v\rangle_N - E(u_H, v); \tag{36}$$

note that $R^u(v) = 0$, $\forall v \in Z_H$.

Step 2. In the second step we compute the adjoints on the working mesh: find $\psi_H = \psi_H^R + i\ \psi_H^I \in Z_H$ such that

$$E(v, \psi_H) = -\ell^{\mathcal{O}}(v), \quad \forall v \in Z_H. \tag{37}$$

We also define the residual

$$R^\psi(v) \equiv -\overline{\ell^{\mathcal{O}}(v)} - \overline{E(v, \psi_H)}; \tag{38}$$

similarly to step 1, $R^\psi(v) = 0$, $\forall v \in Z_H$.

Step 3. In the third step we compute, on the working mesh, the *hybrid fluxes*: find $p_H^u = p_H^{uR} + i\ p_H^{uI} \in \mathcal{Q}_H$ and $p_H^\psi = p_H^{\psi R} + i\ p_H^{\psi I} \in \mathcal{Q}_H$, such that

$$b(v, p_H^u) \;=\; R^u(v), \quad \forall v \in \hat{Z}_H, \tag{39}$$

$$b(v, p_H^\psi) \;=\; R^\psi(v), \quad \forall v \in \hat{Z}_H; \tag{40}$$

we then set $p_H^\pm = \kappa p_H^u \mp p_H^\psi$, where $\kappa \in \mathbb{R}_+$ is a scaling parameter with respect to which we will optimize. The equilibration procedure is a complex version of that developed in [22], which is in turn based on earlier work in the energy–norm context [2, 6, 16].

Step 4. In the fourth step we compute the *reconstructed errors* on the decoupled truth space $\hat{Z}_h$: find $\hat{e}^u = \hat{e}^{uR} + i\ \hat{e}^{uI} \in \hat{Z}_h$ and $\hat{e}^\psi = \hat{e}^{\psi R} + i\ \hat{e}^{\psi I} \in \hat{Z}_h$, such that

$$2E_Y^s(\hat{e}^u, v) - R_H^u(v) + b(v, p_H^u) \;=\; 0, \quad \forall v \in \hat{Z}_h, \tag{41}$$

$$2E_Y^s(\hat{e}^\psi, v) - R_H^\psi(v) + b(v, p_H^\psi) \;=\; 0, \quad \forall v \in \hat{Z}_h; \tag{42}$$

we then set $\hat{e}^\pm = \hat{e}^u \mp \frac{1}{\kappa}\hat{e}^\psi$. It is important to note that equations (41) and (42) correspond to local and uncoupled problems, and are thus very inexpensively solved.

Step 5. Finally, in the fifth step, we compute the lower and upper bounds as

$$s^- \;=\; \Re\{S(u_H)\} - \kappa E_Y^s(\hat{e}^-, \hat{e}^-), \tag{43}$$

$$s^+ \;=\; \Re\{S(u_H)\} + \kappa E_Y^s(\hat{e}^+, \hat{e}^+). \tag{44}$$

As described in [23], these lower and upper bounds can be readily optimized (maximized and minimized, respectively) with respect to the scaling parameter κ by choosing $\kappa = \kappa^*$,

$$\kappa^* = \sqrt{\frac{E^s_Y(\hat{e}^\psi, \hat{e}^\psi)}{E^s_Y(\hat{e}^u, \hat{e}^u)}}. \tag{45}$$

Note that, from (32), κ^* will, necessarily, be real.

3.3 Bounding Properties

In order to prove that the estimators (43) and (44) are (asymptotically) lower and upper bounds respectively for $s_h = \Re\{S(u_h)\}$ (the nonlinear output on the truth mesh), we first introduce the field variable error,

$$e \;=\; u_h - u_H, \tag{46}$$

which is the difference between the truth and working–mesh approximations; note that $e \in Z_h$. We then sum (41) and (42) to obtain the equation for the reconstructed error $\hat{e}^-$

$$2\kappa E^s_Y(\hat{e}^-, v) - \kappa R^u_H(v) - R^\psi_H(v) + b(v, p^-_H) = 0, \quad \forall v \in \hat{Z}_h, \tag{47}$$

in which, since $Z_h \subset \hat{Z}_h$, we can choose $v = e$,

$$2\kappa E^s_Y(\hat{e}^-, e) - \kappa R^u_H(e) - R^\psi_H(e) + b(e, p^-_H) = 0. \tag{48}$$

Appealing to our expressions for R^u_H and R^ψ_H, and noting that $e \in Z_h$ (and hence $b(e, p^-_H) = 0$), we find

$$2\kappa E^s_Y(\hat{e}^-, e) - \kappa\Big[\langle f, e\rangle + \langle g^N, e\rangle_N - E(u_H, e)\Big] + \overline{\ell^{\mathcal{O}}(e)} + \overline{E(e, \psi_H)} = 0. \tag{49}$$

From the usual orthogonality condition we know that $E(e, v) = 0$, $\forall v \in Z_H$, and thus $\overline{E(e, \psi_H)} = 0$. Also, $E(u_h, v) \;=\; \langle f, v\rangle + \langle g^N, v\rangle_N$, $\forall v \in Z_h$, and hence $E(u_h, e) \;=\; \langle f, e\rangle + \langle g^N, e\rangle_N$. We thus obtain

$$2\kappa\overline{E^s_Y(\hat{e}^-, e)} - \kappa E(e, e) + \ell^{\mathcal{O}}(e) = 0, \tag{50}$$

and in particular

$$\Re\Big\{2\kappa\overline{E^s_Y(\hat{e}^-, e)} - \kappa E(e, e) + \ell^{\mathcal{O}}(e)\Big\} = 0. \tag{51}$$

Summing this last identity with (43), applying the Taylor expansion (34), and noting that

$$\Re\{2\overline{E^s_Y(\hat{e}^-, e)}\} = \overline{E^s_Y(\hat{e}^-, e)} + E^s_Y(\hat{e}^-, e) = E^s_Y(e, \hat{e}^-) + E^s_Y(\hat{e}^-, e), \tag{52}$$

we obtain

$$s^- = \Re\{S(u_h)\} - \kappa E^s_Y(e - \hat{e}^-, e - \hat{e}^-) - \kappa E^s_M(e, e) - \Re\{\mathcal{M}(e, e)\}, \tag{53}$$

which is the desired result.

We now note that $\kappa E^s_M(e, e) + \Re\{\mathcal{M}(e, e)\} \leq C \parallel e \parallel_0^2$, which will vanish as $\mathcal{O}(H^4)$ — much faster than $\kappa E^s_Y(e - \hat{e}^-, e - \hat{e}^-)$, which will tend to zero as $\mathcal{O}(H^2)$. It then follows, since E^s_Y is positive–definite, that s^- will approach $\Re\{S(u_h)\}$ from below for H sufficiently small. A similar demonstration can be performed for the upper estimator (asymptotic upper bound) for $\Re\{S(u_h)\}$; in fact, the upper bound is simply the negative of the lower bound for $-S(u_h)$. In particular, we obtain

$$s^+ = \Re\{S(u_h)\} + \kappa E^s_Y(e - \hat{e}^+, e - \hat{e}^+) + \kappa E^s_M(e, e) - \Re\{\mathcal{M}(e, e)\}, \tag{54}$$

from which it is clear that s^+ will approach $\Re\{S(u_h)\}$ from above.

4 Numerical Examples

In this section we present several applications of our procedure. All the examples involve the scattering of a plane wave by a rigid body, and thus there are no essential boundary conditions. We assume that the solution of the problem (1) - (4) is composed of a prescribed incident wave plus a scattered wave, $\tilde{u}_T = \tilde{u}_{(i)} + \tilde{u}$, where the incident wave is of the form $\tilde{u}_{(i)} = \Re\{u_{(i)} e^{i\ (\mathbf{k}^T\mathbf{x}+\omega t)}\}$. We assume that there are no sources in the domain ($\tilde{f} = 0$) and that perfect reflection obtains on the rigid body: $\partial\tilde{u}_T/\partial n = 0$ (or, in terms of the incident wave, $\partial\tilde{u}/\partial n = -\partial\tilde{u}_{(i)}/\partial n$). The complex Helmholtz equation is thus: find $u : \bar{\Omega} \to \mathbb{C}$ such that

$$\begin{aligned}
-\nabla^2 u - k^2 u &= 0 && \text{in} \quad \Omega, && (55)\\
\frac{\partial u}{\partial n} &= -i\ \mathbf{k}^T\hat{\mathbf{n}}\ u_{(i)}\ e^{i\ \mathbf{k}^T\mathbf{x}} && \text{on} \quad \Gamma_N, && (56)\\
\frac{\partial u}{\partial n} &= -i\ k\ u && \text{on} \quad \Gamma_R, && (57)
\end{aligned}$$

where k denotes the modulus of $\mathbf{k}$. The corresponding weak form is simply (14) with $f = g^D = 0$ and $g^N = -i\ \mathbf{k}^T\mathbf{n}\ u_{(i)}\ e^{i\ \mathbf{k}^T\mathbf{x}}$.

In the following examples we apply our procedure to three different engineering outputs. The first output is the normalized L^2 norm of the solution

$$S_1(v) = \frac{1}{A_\Omega}\int_\Omega v\bar{v}\ d\Omega, \tag{58}$$

where A_Ω is the area of the domain. To identify $\ell^{\mathcal{O}}$ we appeal to (34),

$$S_1(u_H + w) = \frac{1}{A_\Omega}\int_\Omega (u_H + w)\overline{(u_H + w)}\ d\Omega = S_1(u_H) + \frac{1}{A_\Omega}\int_\Omega [u_H\overline{w} + \overline{u}_H w]\ d\Omega + S_1(w), \tag{59}$$

and thus

$$\ell^{\mathcal{O}}(w) = \frac{2}{A_\Omega}\int_\Omega \overline{u}_H w\ d\Omega, \qquad \mathcal{M}(w,w) = S_1(w). \tag{60}$$

The second output is the modulus squared over a boundary strip $\Gamma^{\mathcal{O}}$,

$$S_2(v) = \frac{1}{l_{\Gamma^{\mathcal{O}}}}\int_{\Gamma^{\mathcal{O}}} v\bar{v}\ d\Gamma, \tag{61}$$

where $l_{\Gamma^{\mathcal{O}}}$ is the length of the boundary strip. This definition yields

$$\ell^{\mathcal{O}}(w) = \frac{2}{l_{\Gamma^{\mathcal{O}}}}\int_{\Gamma^{\mathcal{O}}} \overline{u}_H w\ d\Gamma, \qquad \mathcal{M}(w,w) = S_2(w). \tag{62}$$

The third output is the real part of the solution, and thus

$$S_3(v) = \int_\Omega v\ d\Omega, \tag{63}$$

and $\ell^{\mathcal{O}}(w) = S_3(w)$, $\mathcal{M}(w,w) = 0$.

We consider a square domain in which an incident plane wave is travelling in the negative y direction; inside this region there is a rigid body that scatters the incident wave. We impose the radiation condition (57) on the exterior boundary and the reflection condition (56) on the rigid body surface. The boundary strip on which the output (61) is evaluated is the segment

$\Gamma^{\mathcal{O}} = [(0.5, 1.0), (0.8, 1.0)]$. The geometry of the domain, the boundary conditions, and the direction of the incident wave are depicted in Figure 2.

We introduce triangulations $\mathcal{T}_{H_0,R}$ ($R = 1, 2, 4, 8, 16$) that are uniform refinements of the coarsest mesh, $\mathcal{T}_{H_0,1}$; even in $\mathcal{T}_{H_0,1}$ we introduce smaller elements near the rigid body to prevent dominance of the corner singularities. The truth mesh corresponds to $\mathcal{T}_{H_0,16}$; the working meshes correspond to $\mathcal{T}_{H_0,R}$ ($R = 1, 2, 4, 8$), for which we denote the effective element size as $H \equiv 1/R$. Figure 3.a and Figure 3.b show $\mathcal{T}_{H_0,1}$ and $\mathcal{T}_{H_0,16}$ respectively; Figure 3.c shows graphically the decoupled truth mesh which, in effect, defines $\hat{Z}_h$. Note that, for the refinement values R chosen, $Z_H \subset Z_h \subset Z$ as required by the theory. In order to demonstrate the dependence of the results on the wave number, we consider three wave number values: $k = \pi$, $k = 3\pi$, and $k = 5\pi$. It is important to note that the coarsest mesh, $\mathcal{T}_{H_0,1}$, is not sufficiently fine to capture even the incident wave for $k = 3\pi$ or $k = 5\pi$.

We first compute the solution on the truth mesh, u_h, from which we can then evaluate the corresponding truht output, s_h; recall that we assume s_h differs negligibly from the exact value of the output, s. The columns of Figure 4 show the real part, the imaginary part, and the modulus of the scattered wave, as well as the modulus of total wave, for the three wave numbers considered. In actual practice we would not, of course, have access to u_h; we indulge here to demonstrate that s^+ and s^- are, indeed, bounds for s_h.

Next, based on $\mathcal{T}_{H_0,R}$ for $R = 1, 2, 4, 8$, we compute the working mesh output s_H, the lower bound estimator s^- (43), the upper bound estimator s^+ (44), the bound–predicted nonlinear output value $s_H^{pre} = 1/2(s^+ + s^-)$, and the (half) bound gap, $\Delta(\mathcal{T}_H) = 1/2(s_h^+ - s_h^-)$, for each of the outputs (58), (61) and (63) and each of the three wave numbers considered. In actual practice $\Delta(\mathcal{T}_H)$, which requires computations only on the decoupled fine mesh, would serve as the error bound on s_H^{pre} (or s_H); even more directly, s^- and s^+ would serve as delimiters for the range in which s_h must lie (at least for H sufficiently small). Often, depending on the particular problem, either the upper or the lower bound will be more relevant to the engineering design procedure.

Figures 5 presents, for the output $S_1(u)$ and for each of the wave numbers, s^-/s_h, s^+/s_h, s_H^{pre}/s_h and s_H/s_h as function of H. The same plots are presented in Figures 6 and 7 for outputs $S_2(u)$ and $S_3(u)$ respectively. We observe that bounds obtain even for the largest values of H (in which there is not clearly enough resolution for the $k = 3\pi$ and $k = 5\pi$ waves). As expected, the bounds are less sharp with increasing wave number; for higher wave numbers a finer mesh is needed. This behaviour can be better observed in Figure 8, in which we plot the (half) bound gap, $\Delta(\mathcal{T}_h)$, as function of H. Notice that quadratic converge is obtained, as might be expected from equations (53) and (54) and earlier theory for the coercive case [18].

In order to demonstrate the influence of the initial mesh on the accuracy of the bounds, we repeat the bound calculations for the output (61), for $k = \pi$, for an initial mesh $\mathcal{T}_{H_0,1}$ which is modestly refined near $\Gamma^{\mathcal{O}}$. Figure 9.a depicts the initial mesh $\mathcal{T}_{H_0,1}$; Figure 9.b shows the new values for s^-/s_h, s^+/s_h, s_H^{pre}/s_h, and s_H/s_h. Better bounds are obtained since the adjoint is more accurately approximated; the technique of [23] will automatically produce such an *output–optimal* mesh.

5 Conclusions

The general formulation for *a posteriori* bounds for output functionals of partial diferential equations has been extended to nonlinear outputs of multidimensional complex exterior Helmholtz problems. In particular, it has been proven that the estimators obtained are asymptotically lower and upper bounds for the *exact* output (or more precisely, the truth output, s_h). Numerical examples verify the predicted quadratic convergence; furthermore, even for the largest value of H, strict bounds are obtained, indicating that the *asymptotic* qualifier is, in fact, rather weak. In many cases the bounds are sufficiently sharp that relatively coarse meshes produce acceptable results; whereas typically the coarse mesh would not be trusted, the error bounds permit their safe application — thus providing both certainty and efficiency. Efficiency can be further improved by considering the adaptive procedures of [23].

Acknowledgements

This work was supported by NASA Grants NAG1–1978, NAG1–1587 and NAG4–105, DARPA and ONR Grant N00014–91-J-1889, and AFOSR Grant F49620–97–1–0052. J. Sarrate has been supported by the *Comissionat per a Universitats i Recerca* of the *Generalitat de Catalunya.*

Appendix

We show here how our bound formulation can also be developed in terms of product spaces of real functions. To begin, we consider the product space $H^1(\mathcal{D}) \times H^1(\mathcal{D})$, and define

$$\tilde{X}(\mathcal{D}) = \Big\{(\alpha,\beta) \in H^1(\mathcal{D}) \times H^1(\mathcal{D}) :\ \alpha + i\beta \in \tilde{Z}(\mathcal{D})\Big\}, \tag{64}$$

and similarly

$$X = \Big\{(\alpha,\beta) \in \tilde{X}(\Omega) :\ \alpha + i\beta \in Z\Big\}, \tag{65}$$

$$X^D = \Big\{(\alpha,\beta) \in \tilde{X}(\Omega)\ :\ \alpha + i\beta \in Z^D\Big\}. \tag{66}$$

We then define a bilinear form: $\mathcal{B} : \tilde{X}(\Omega) \times \tilde{X}(\Omega) \to \mathbb{R}$ as

$$\begin{aligned}\mathcal{B}((\alpha,\beta),\ (\phi,\mu)) \ \equiv\ & a(\alpha,\phi) + a(\beta,\mu) - m(\alpha,\phi) - m(\beta,\mu) + p(\alpha,\mu) - p(\beta,\phi) \\ -\ & \langle f^R,\phi\rangle - \langle f^I,\mu\rangle - \langle g^{NR},\phi\rangle_N - \langle g^{NI},\mu\rangle_N,\end{aligned} \tag{67}$$

where the bilinear forms (16) - (18) and duality pairings (19) - (20) are now defined for real functions. The solution of problem (14), $u = u^R + iu^I$, can thus be found by solving the following problem: find $(u^R, u^I) \in X^D$ such that

$$\mathcal{B}((u^R,u^I),\ (\phi,\mu)) = 0, \quad \forall\ (\phi,\mu) \in X. \tag{68}$$

To see that (68) and (14) are, in fact, equivalent, we note that if we set $\phi = v^R$ and $\mu = v^I$, (68) reduces to the real part of (14); whereas if we set $\phi = -v^I$ and $\mu = v^R$, then (68) reduces to the imaginary part of (14). From this point of view, we understand that problem (14) contains some redundancy, since the real and imaginary parts of the equation must be satisfied for the real and imaginary parts of the test functions.

In order to interpret the five steps of the procedure (35) - (44) in terms of spaces of real functions, we first need to introduce the definitions of the equivalent real spaces. Analogously to Z_δ, Z_δ^D, and $\hat{Z}_\delta$, (21), (22), and (25), we define

$$X_\delta = \Big\{(\alpha,\beta)\ :\ \alpha|_{T_\delta} \in \mathbf{P}_1(T_\delta),\ \beta|_{T_\delta} \in \mathbf{P}_1(T_\delta),\ \forall T_\delta \in \mathcal{T}_\delta\ \Big\} \cap X, \tag{69}$$

$$X_\delta^D = \Big\{(\alpha,\beta)\ :\ \alpha|_{T_\delta} \in \mathbf{P}_1(T_\delta),\ \beta|_{T_\delta} \in \mathbf{P}_1(T_\delta),\ \forall T_\delta \in \mathcal{T}_\delta\ \Big\} \cap X^D, \tag{70}$$

$$\hat{X}_\delta = \Big\{(\alpha,\beta)|_{T_H} \in \tilde{X}(T_H),\ \forall T_H \in \mathcal{T}_H\ :\ \alpha|_{T_\delta} \in \mathbf{P}_1(T_\delta),\ \beta|_{T_\delta} \in \mathbf{P}_1(T_\delta),\ \forall T_\delta \in \mathcal{T}_\delta\ \Big\}. \tag{71}$$

We also define the real counterpart of the space $\mathcal{Q}_H$ as $Q_H = W_H \times W_H$, where

$$W_H = \Big\{ q : \ q|_\gamma \in \mathbf{P}_1(\gamma), \ \forall \gamma \in \mathcal{E}(\mathcal{T}_H), \text{ and } \ q|_{\Gamma_N} = q|_{\Gamma_R} = 0 \Big\}. \tag{72}$$

The continuity bilinear form $b(\cdot,\cdot)$ of (27) is also now defined over real functions as $b : \hat{X}_h \times Q_H \to \mathbb{R}$, where

$$b((\alpha,\beta),(q_\alpha,q_\beta)) = \sum_{\gamma\in\mathcal{E}(\mathcal{T}_H)} \int_\gamma [\alpha]_\gamma \, q_\alpha|_\gamma \, d\Gamma \ + \ \int_\gamma [\beta]_\gamma \, q_\beta|_\gamma \, d\Gamma. \tag{73}$$

It remains only to modify properly the definition of the nonlinear output: we set $s = \breve{S}((\alpha,\beta))$, where $\breve{S} : \tilde{X}(\Omega) \to \mathbb{R}$ such that $\breve{S}((\alpha,\beta)) = \Re\{S(\alpha + i\beta)\}$.

This problem is now defined over spaces of real functions and the bound formulation presented in [19] is directly applicable. Following that notation, and since $\mathcal{B}$ is bilinear, we have

$$E((\alpha,\beta), \ (\phi,\mu)) = a(\alpha,\phi) + a(\beta,\mu) - m(\alpha,\phi) - m(\beta,\mu) + p(\alpha,\mu) - p(\beta,\phi). \tag{74}$$

As usual, we decompose E into its symmetric and skew–symmetric parts, $E = E^s + E^a$, where

$$\begin{aligned} E^s((\alpha,\beta), \ (\phi,\mu)) \ &\equiv \ a(\alpha,\phi) + a(\beta,\mu) - m(\alpha,\phi) - m(\beta,\mu), &(75)\\ E^a((\alpha,\beta), \ (\phi,\mu)) \ &\equiv \ p(\alpha,\mu) - p(\beta,\phi). &(76)\end{aligned}$$

The symmetric part is then further decomposed as $E^s \equiv E^s_Y + E^s_M$, where

$$\begin{aligned} E^s_Y((\alpha,\beta), \ (\phi,\mu)) \ &\equiv \ a(\alpha,\phi) + a(\beta,\mu), &(77)\\ E^s_M((\alpha,\beta), \ (\phi,\mu)) \ &\equiv \ -m(\alpha,\phi) - m(\beta,\mu). &(78)\end{aligned}$$

Finally, we write

$$\breve{S}((u^R,u^I) + (\alpha,\beta)) \ = \ \breve{S}((u^R,u^I)) + \breve{\ell}^{\mathcal{O}}((\alpha,\beta)) + \breve{\mathcal{M}}((\alpha,\beta),(\alpha,\beta)), \tag{79}$$

such that $\breve{\ell}^{\mathcal{O}}((\alpha,\beta)) = \Re\{\ell^{\mathcal{O}}(\alpha + i\beta)\}$, and $\breve{\mathcal{M}}((\alpha,\beta),(\alpha,\beta)) = \Re\{\mathcal{M}(\alpha + i\beta, \alpha + i\beta)\}$.

With these definitions, the estimator procedure comprises the following five steps.

Step 1. Compute the finite element solution $(u^R_H, \ u^I_H) \in X^D_H$ such that

$$\begin{aligned} E((u^R_H, \ u^I_H), \ (\phi,\mu)) \ &= \ \langle f^R, \phi\rangle + \langle f^I, \mu\rangle \\ &+ \ \langle g^{NR}, \phi\rangle_N + \langle g^{NI}, \mu\rangle_N, \quad \forall(\phi,\mu) \in X_H. &(80)\end{aligned}$$

We also define the residual

$$R^u(\phi,\mu) \equiv \langle f^R, \phi\rangle + \langle f^I, \mu\rangle + \langle g^{NR}, \phi\rangle_N + \langle g^{NI}, \mu\rangle_N - E((u^R_H, \ u^I_H), \ (\phi,\mu)). \tag{81}$$

Step 2. Compute the adjoints $(\psi^R_H, \ \psi^I_H) \in X_H$ such that

$$E((\phi,\mu), \ (\psi^R_H, \ \psi^I_H)) = -\breve{\ell}^{\mathcal{O}}((\phi,\mu)), \quad \forall(\phi,\mu) \in X_H. \tag{82}$$

We also define the residual

$$R^\psi(\phi,\mu) \equiv -\breve{\ell}^{\mathcal{O}}((\phi,\mu)) - E((\phi,\mu), \ (\psi^R_H, \ \psi^I_H)). \tag{83}$$

Step 3. Compute the *hybrid fluxes* $(p_H^{uR}, p_H^{uI}) \in Q_H$, and $(p_H^{\psi R}, p_H^{\psi I}) \in Q_H$, such that

$$\begin{aligned} b((\phi,\mu),\ (p_H^{uR}, p_H^{uI})) &= R^u(\phi,\mu), \quad \forall (\phi,\mu) \in \hat{X}_H, && (84)\\ b((\phi,\mu),\ (p_H^{\psi R}, p_H^{\psi I})) &= R^\psi(\phi,\mu), \quad \forall (\phi,\mu) \in \hat{X}_H; && (85) \end{aligned}$$

we then set $(p_H^{\pm R}, p_H^{\pm I}) = \kappa(p_H^{uR}, p_H^{uI}) \mp (p_H^{\psi R}, p_H^{\psi I})$, where $\kappa \in \mathbb{R}_+$ is our scaling parameter.

Step 4. Compute the reconstructed errors: find $(\hat{e}^{uR}, \hat{e}^{uI}) \in \hat{X}_h$ and $(\hat{e}^{\psi R}, \hat{e}^{\psi I}) \in \hat{X}_h$ such that

$$\begin{aligned} 2E_Y^s((\hat{e}^{uR}, \hat{e}^{uI}), (\phi,\mu)) - R_H^u(\phi,\mu) + b((\phi,\mu), (p_H^{uR}, p_H^{uI})) &= 0, \quad \forall (\phi,\mu) \in \hat{X}_h, && (86)\\ 2E_Y^s((\hat{e}^{\psi R}, \hat{e}^{\psi I}), (\phi,\mu)) - R_H^\psi(\phi,\mu) + b((\phi,\mu), (p_H^{\psi R}, p_H^{\psi I})) &= 0, \quad \forall (\phi,\mu) \in \hat{X}_h; && (87) \end{aligned}$$

we then set $(\hat{e}^{\pm R}, \hat{e}^{\pm I}) = (\hat{e}^{uR}, \hat{e}^{uI}) \mp \frac{1}{\kappa}(\hat{e}^{\psi R}, \hat{e}^{\psi I})$.

Step 5. Compute lower and upper bounds

$$\begin{aligned} s^- &= \check{S}((u_H^R,\ u_H^I)) - \kappa E_Y^s((\hat{e}^{-R}, \hat{e}^{-I}),\ (\hat{e}^{-R}, \hat{e}^{-I})), && (88)\\ s^+ &= \check{S}((u_H^R,\ u_H^I)) + \kappa E_Y^s((\hat{e}^{+R}, \hat{e}^{+I}),\ (\hat{e}^{+R}, \hat{e}^{+I})). && (89) \end{aligned}$$

As it has been proved in [19] for real function spaces, these lower and upper estimators are, in fact, upper and lower bounds for $\check{S}((u_h^R, u_h^I))$ for H sufficiently small.

References

[1] R.A. Adams, *Sobolev Spaces*, Academic Press, New York, 1975.

[2] M. Ainsworth and J.T. Oden, 'A unified approach to a posteriori error estimation using element residual methods', Numer. Math., **65**, 23–50, (1993).

[3] M. Ainsworth and J.T. Oden, 'A posteriori error estimation in finite element analysis', Comp. Meth. Appl. Mech. Engrg., **142**, 1-88 (1997).

[4] S. Amini and K. Chen, 'Iterative solution of boundary element equations for the exterior acoustic problem', J. Vibr. Acoust. **112**, 257–262, (1990).

[5] I. Babuška, F. Ihlenburg, T. Strouboulis and S.K. Gangaraj, 'A posteriori error estimator for finite element solutions of Helmholtz equation, Part II: Estimation of the pollution error', Int. J. Numer. Methods Engrg. **40**, pp. 3883–3900, (1997).

[6] R.E. Bank and A. Weiser, 'Some a posteriori error estimators for elliptic partial differential equations', Math. Comp., **44**:170, 283–301, (1985).

[7] R. Becker and R. Rannacher, 'Weighted a posteriori error control in finite element methods', IWR Preprint 96–1 (SFB 359), Heidelberg, (1996).

[8] P. Bettess, 'Infinite elements', Int. J. Numer. Methods Engrg., **11**, 53–64, (1977)

[9] M.O. Bristeau, R. Glowinsky and J. Périaux, 'Using exact controllability to solve the Helmholtz equation at high wave numbers', in: Proc. 2nd. Int. Conf. on Math. and Num. Aspects of Wave Propagation, SIAM, (1993).

[10] L. Demkowicz, J.T. Oden, 'Recent progres on application of hp–adaptive BE/FE methods to elastic scattering', Int. J. Numer. Methods Engrg., **37**, 2893–2910, (1994).

[11] F. Ihlenburg and I. Babuška, 'Finite element solution of the Helmholtz equation with high wave number, Part I: the h-version of the FEM', Computers Math. Applic., **30**:9, 9–37, (1995).

[12] D. Givoli and J.B. Keller, 'Non–refecting boundary conditions for elastic waves', Wave Motion, **12**, 261–279, (1990).

[13] C. Johnson and P. Hansbo, 'Adaptive finite element methods in computational mechanics', Comp. Meth. Appl. Mech. Engrg., **101**, 143-181, (1992).

[14] M. Kamon, M.J. Tsuk and J.K. White, 'FASTHENRY: A multipole–accelerated 3–D inductance extraction program', IEEE Trans. Microwave Theory Tech., **42**, 1750–1758, (1994).

[15] K. Kashiyama and M. Sakuraba, 'Adaptive boundary-type finite element method for wave diffraction-refraction in harbours', Comp. Meth. Appl. Mech. Engrg., **112**, 185–197, (1994).

[16] P. Ladeveze and D. Leguillon, 'Error estimation procedures in the finite element method and applications', SIAM J. Numer. Anal., **20**, 485–509, (1983).

[17] L. Machiels, A.T. Patera, J. Peraire and Y. Maday, 'A general Framework for finite element a posteriori error control: application to linear and nonlinear convection–dominated problems', ICFD Conference on Numerical Methods for Fluid Dynamics, Oxford, England, 1998.

[18] Y. Maday and A.T. Patera, 'Numerical analysis of a posteriori finite elements bounds for linear–functional outputs', Mathematical Models and Methods in Applied Science, submitted.

[19] Y. Maday, A.T. Patera and J. Peraire, 'A general formulation for a posteriori bounds for output functionals of partial differential equations; application to the eigenvalue problem', C. R. Acad. Sci. Paris, to appear.

[20] M. Paraschivoiu, *A Posteriori Finite Element Bounds for Linear–Functional Outputs of Coercive Partial Dfferential Equations and of the Stokes Problem*, Ph.D. Thesis, Department of Mechanical Engineering, M.I.T., October, 1997.

[21] M. Paraschivoiu and A.T. Patera, 'A posteriori bounds for linear–functional outputs of Crouzeix–Raviart finite element discretizations of the incompressible Stokes problem', Int. J. for Num. in Fluids, submitted.

[22] M. Paraschivoiu, J. Peraire and A.T. Patera, 'A posteriori finite element bounds for linear–functional outputs of elliptic partial differential equations', Comp. Meth. Appl. Mech. Engrg. **150**, 289-312 (1997).

[23] J. Peraire and A.T. Patera, 'Bounds for linear–functionals outputs of coercive partial differential equations: local indicators and adaptive refinement', in Proceedings of the Workshop on New Advances in Adaptive Computational Methods in Mechanics, Cachan, France, eds. P. Ladeveze and J.T. Oden, Elsevier, 1997.

[24] J. Peraire and A.T. Patera, 'Asymptotic a posteriori finite element bounds for the outputs of non coercive problems: the Helmholtz and Burgers equations', Comp. Meth. Appl. Mech. Engrg., to appear.

[25] Y. Saad and M.H. Schultz, 'GMRES: A generalized minimal residual algorithm for solving nonsymmetric linear systems', SIAM J. Scientific Statistical Computing, **7**, 856–869, (1986).

[26] A.H. Schatz, 'An observation concerning Ritz–Galerkin methods with indefinite bilinear forms', Math. Comp., **28**:128, 959–962, (1974).

[27] J.R Stewart, *Adaptive Finite Element Method for the Helmholtz Equation in Exterior Domains*, Ph.D. Thesis, Division of Applied Mechanics, Stanford University, Stanford, CA, 1995.

[28] J.R Stewart and J.R. Hughes, 'Explicit residual–based a posteriori error estimation for finite element discretizations of the Helmholtz equation: Computation of the constant and new measures of the error estimator quality', Comp. Meth. Appl. Mech. Engrg., **131**, 335-363, (1996).

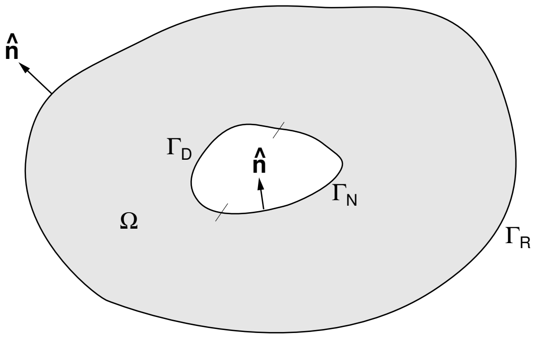

Figure 1: General geometry and boundary conditions for the complex Helmholtz problem.

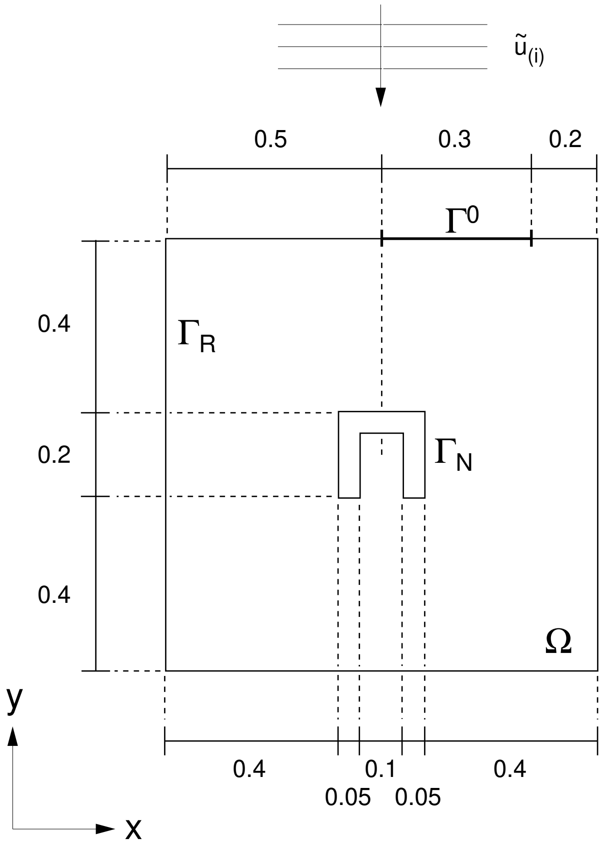

Figure 2: Geometry and boundary conditions for two–dimensional plane wave scattering by a rigid body.

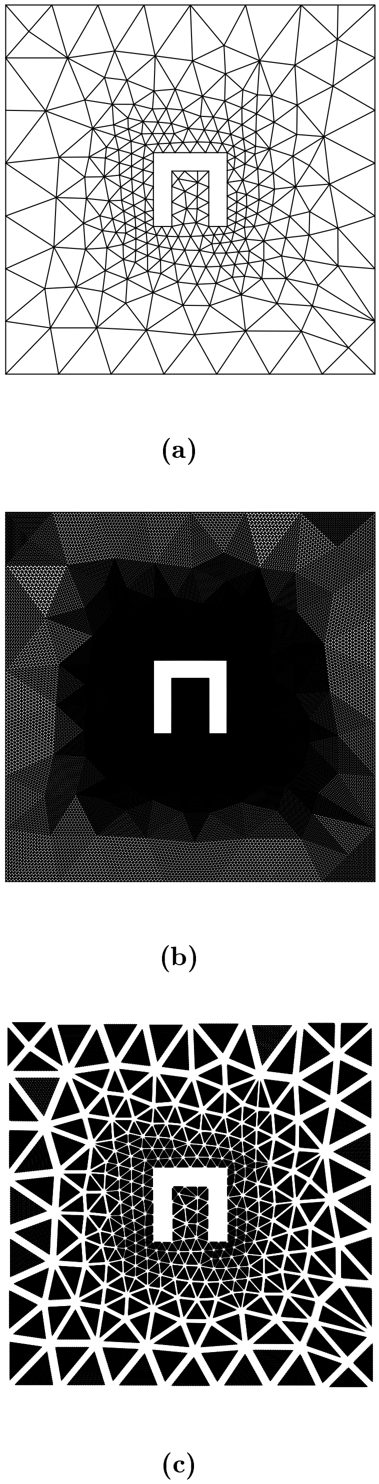

Figure 3: **(a)** Coarsest mesh $\mathcal{T}_{H_0,1}$. **(b)** Finest mesh $\mathcal{T}_{H_0,16}$. **(c)** Mesh corresponding to the *broken* space $\hat{Z}_h$.

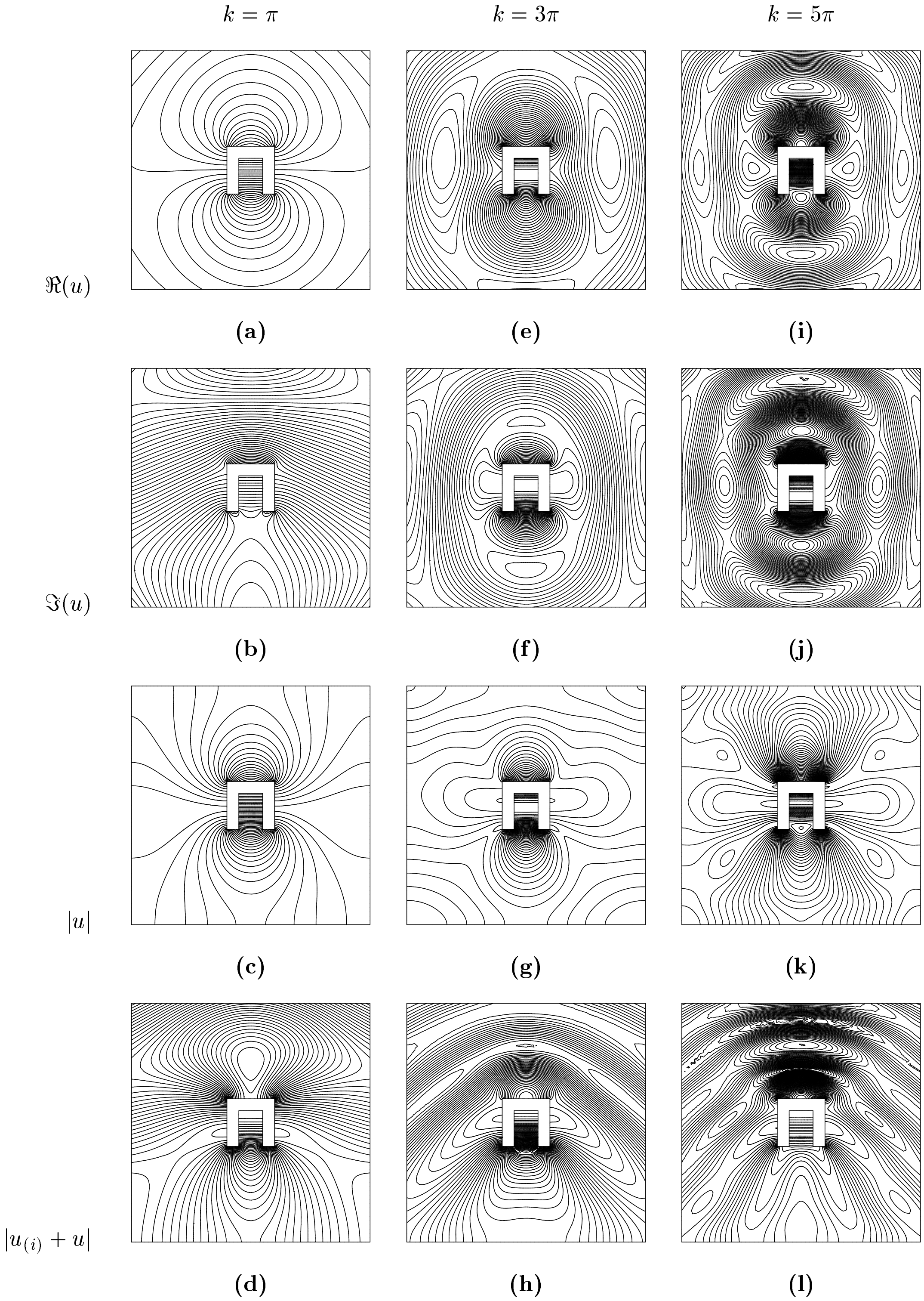

Figure 4: Contours plots of: $\Re(u)$ for **(a)** $k = \pi$, **(e)** $k = 3\pi$, and **(i)** $k = 5\pi$; $\Im(u)$ for **(b)** $k = \pi$, **(f)** $k = 3\pi$, and **(j)** $k = 5\pi$; $|u|$ for **(c)** $k = \pi$, **(g)** $k = 3\pi$, and **(k)** $k = 5\pi$; and $|u_{(i)} + u|$ for **(d)** $k = \pi$, **(h)** $k = 3\pi$, and **(l)** $k = 5\pi$.

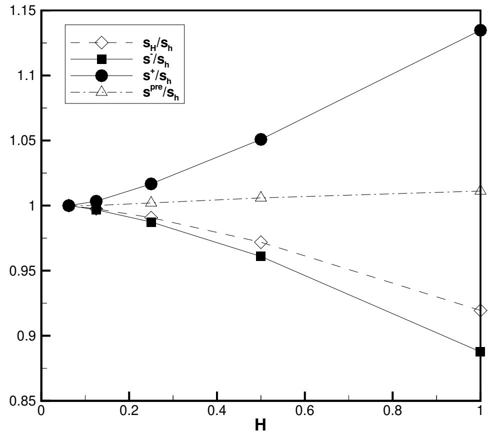

(a)

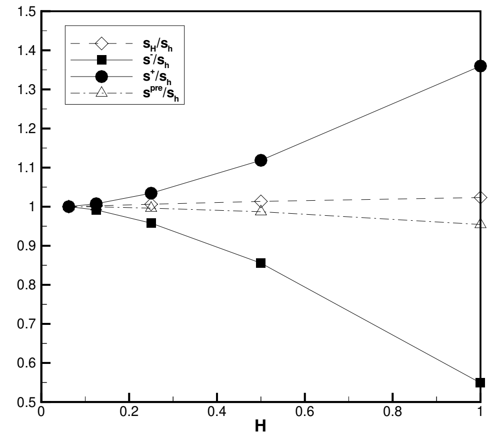

(b)

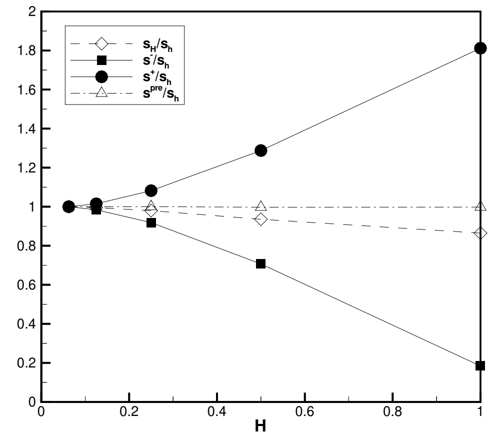

(c)

Figure 5: Plots of s^-/s_h, s^+/s_h, s_H^{pre}/s_h and s_H/s_h for $S_1(u)$ and **(a)** $k = \pi$, **(b)** $k = 3\pi$, and **(c)** $k = 5\pi$.

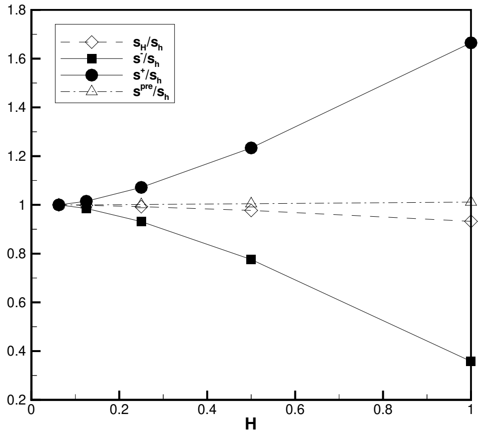

(a)

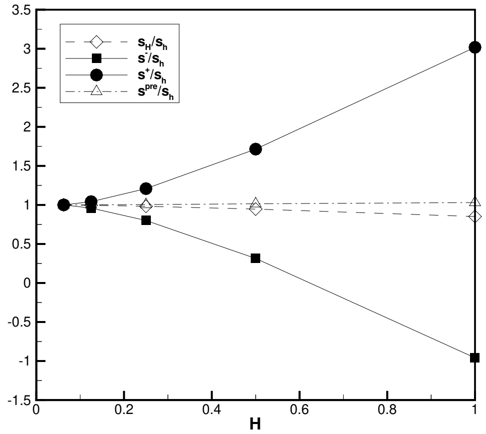

(b)

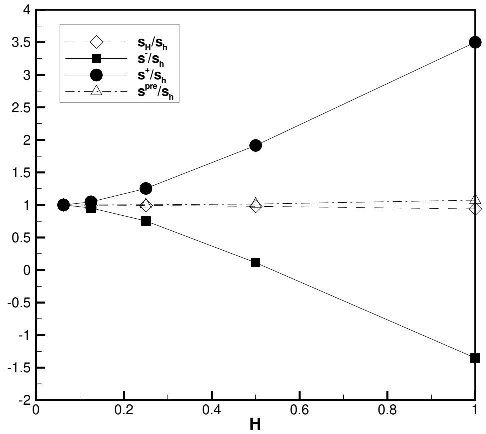

(c)

Figure 6: Plots of s^-/s_h, s^+/s_h, s_H^{pre}/s_h and s_H/s_h for $S_2(u)$ and **(a)** $k = \pi$, **(b)** $k = 3\pi$, and **(c)** $k = 5\pi$.

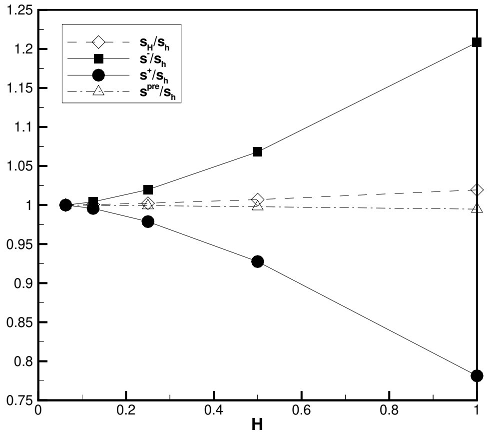

(a)

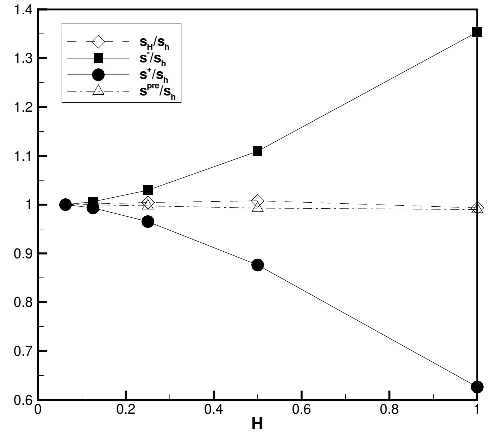

(b)

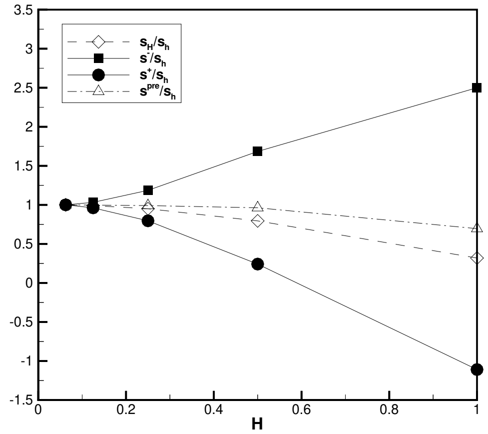

(c)

Figure 7: Plots of s^-/s_h, s^+/s_h, s_H^{pre}/s_h and s_H/s_h for $S_3(u)$ and **(a)** $k = \pi$, **(b)** $k = 3\pi$, and **(c)** $k = 5\pi$. Note that $\Re\{S_3(u)\}$ is negative, and hence the bounds *appear* reversed.

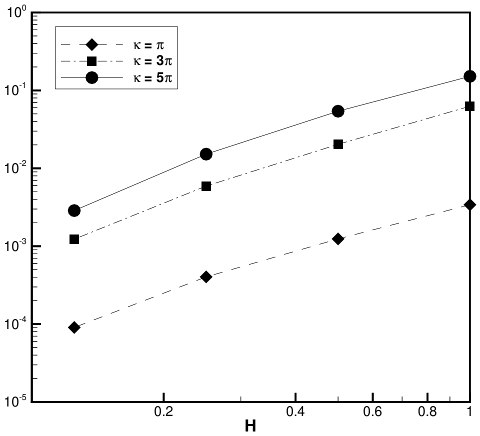

(a)

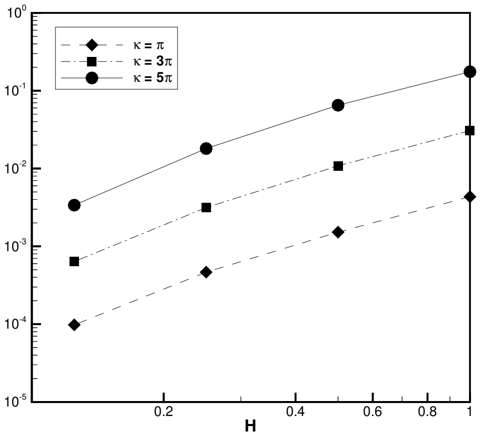

(b)

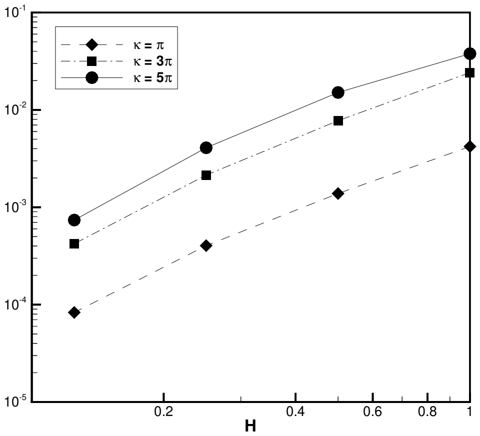

(c)

Figure 8: Plots of $\Delta(\mathcal{T}_h)$ for **(a)** $S_1(u)$, **(b)** $S_2(u)$, and **(c)** $S_3(u)$.

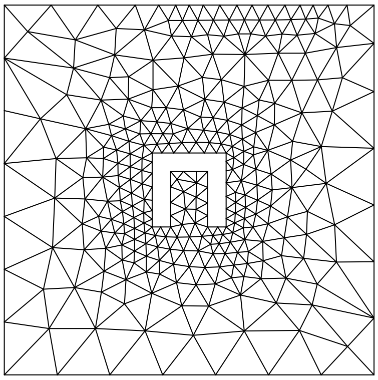

(a)

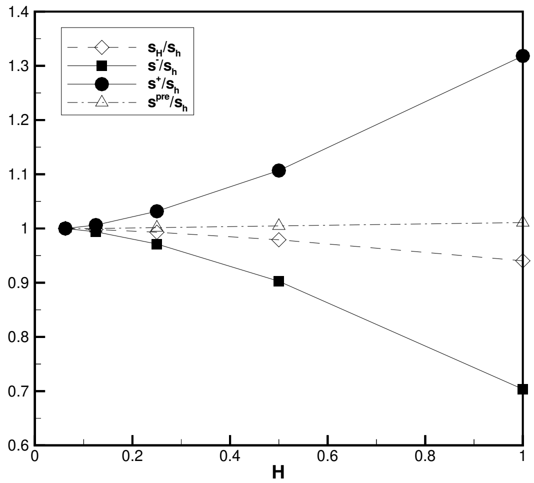

(b)

Figure 9: **(a)** Modified mesh. **(b)** Plots of s^-/s_h, s^+/s_h, s_H^{pre}/s_h and s_H/s_h for $S_2(u)$ and $k = \pi$ for the modified mesh.